



# V-doped TiO<sub>2</sub> photocatalysts and their application to pollutant degradation

Lucía Rossi<sup>1</sup> · Magdalena Palacio<sup>1</sup> · Paula I. Villabrille<sup>1</sup> · Janina A. Rosso<sup>2</sup>

Received: 13 July 2020 / Accepted: 1 January 2021 / Published online: 20 January 2021

© The Author(s), under exclusive licence to Springer-Verlag GmbH, DE part of Springer Nature 2021

## Abstract

V-doped TiO<sub>2</sub> materials (0.01, 0.05, 0.10, and 1.00 nominal atomic %) were synthesized by the sol-gel method and characterized by X-ray diffraction, Raman spectroscopy, UV–visible diffuse reflectance spectroscopy, N<sub>2</sub> adsorption–desorption isotherms, X-ray photoelectron spectroscopy, and H<sub>2</sub>-temperature programmed reduction. Two vanadium precursors (vanadyl acetylacetonate and ammonium metavanadate) and three calcination temperatures (400, 500, and 600 °C, with and without air circulation) were assayed. The efficiency of the materials as photocatalysts was studied by the degradation of phenol with UV and visible lamps. The photocatalyst prepared from vanadium acetylacetonate, with a vanadium content of 0.01 nominal atomic %, calcination at 400 °C without air circulation (0.01VTi-400), showed the best performance, reaching 100% and 30% degradation of phenol (50 μM) by irradiation with UV lamps (3 h) and visible lamps (5 h), respectively. To evaluate the efficiency of this catalyst in the degradation of other structurally related compounds, two substituted phenols were selected: 4-chlorophenol and 4-nitrophenol. The 0.01VTi-400 photocatalyst showed to be applicable to the degradation of phenolic compounds when the substituent was an activating group or a weakly deactivating group (for electrophilic reactions). Additionally, the selectivity of 0.01VTi-400 for phenol degradation in the presence of Aldrich humic acid was tested: phenol degradation reached 68% (3 h, UV lamps). The performance of 0.01VTi-400 indicated that it is a promising material for further applications.

**Keywords** Vanadyl acetylacetonate · Ammonium metavanadate · Phenol · 4-chlorophenol · 4-nitrophenol · Aldrich humic acid

## Introduction

Increased discharges of inadequately treated wastewater have been detrimental to water quality around the world. Phenolic compounds are a family of wastewater pollutants produced by different activities, such as biotechnological and chemical industries, petroleum refineries, food processing, and

production of herbicides and fungicides (Patel et al. 2014). They can be found in a wide range of concentrations from 0.1 to 4000 mg L<sup>-1</sup> (Sas et al. 2018; Tolosana-Moranchel et al. 2019).

In particular, phenol was found in some refinery wastewater samples in concentrations up to 15 mg L<sup>-1</sup> (El-naas et al. 2014). Phenols are considered priority pollutants due to their high toxicity and nonbiodegradable properties, so different world organizations have regulated their discharge. According to the US Environmental Protection Agency, the phenolic content in wastewater should be less than 1 mg L<sup>-1</sup> (Sas et al. 2018). Finding an efficient and sustainable method for the degradation of phenols from wastewater remains a challenge.

Photocatalysis has shown a high potential for removing pollutants from aqueous media (Fujishima et al. 2008; Dong et al. 2015). The photocatalytic mechanism is mainly based on the lighting of a semiconductor with energy greater than the band gap energy (E<sub>bg</sub>) to produce charge carriers (electrons in the conduction band and holes in the valence band). The

---

Responsible Editor: Sami Rtimi

✉ Paula I. Villabrille  
paulav@conicet.gov.ar

<sup>1</sup> CINDECA (CONICET-CIC-UNLP), Dto. de Química, Facultad de Ciencias Exactas, Universidad Nacional de La Plata, Calle 47 N° 257, 1900 La Plata, Buenos Aires, Argentina

<sup>2</sup> INIFTA (UNLP-CONICET), Dto. de Química, Facultad de Ciencias Exactas, Universidad Nacional de La Plata, Blvd. 113 y 64, 1900 La Plata, Buenos Aires, Argentina

photoinduced process mainly generates hydroxyl radicals ( $\text{HO}^\bullet$ ), which are primarily responsible for the oxidation reactions of organic pollutants (Schneider et al. 2014).  $\text{TiO}_2$  (E<sub>g</sub> for anatase  $\text{TiO}_2$ : 3.2 eV, for rutile  $\text{TiO}_2$ : 3.0 eV) is one of the most widely used semiconductors in heterogeneous photocatalysis because of its high reactivity, strong oxidizing power, thermal stability, and low toxicity (Hoffmann et al. 1995; Hernández-Alonso et al. 2009).

Reactions photocatalyzed by  $\text{TiO}_2$  are nonselective oxidations because they are governed by free-radical reaction mechanisms. Low selectivity means that the efficacy of the treatment could be strongly inhibited in effluents containing low concentrations of pollutants (highly toxic substances) together with high concentrations of natural organic matter (NOM) (Palacio et al. 2017). NOM usually leads to the loss of oxidizing capacity in a radical-based advanced oxidation process (Deng et al. 2017; Song et al. 2017; Cai et al. 2021). Tang et al. (2018) presented some evidence on the effect of humic acid as  $\text{HO}^\bullet$  scavenger hindering  $\text{TiO}_2$  activity for the photocatalytic removal of organic phosphate esters. Then, evaluating the effect of NOM, a ubiquitous component of the water matrix, becomes another requirement for the application of a photocatalytic treatment.

$\text{TiO}_2$  modification with noble, transition, or rare earth metals has shown enormous potential to overcome the limitations of visible light absorption and high charge carrier recombination, which are two limitations of  $\text{TiO}_2$  particles (Zaleska 2008). Several theoretical and experimental studies indicated that metal doping improves the photocatalytic activity of  $\text{TiO}_2$ , reducing the value of its E<sub>g</sub> or introducing energy levels from impurities (Zhao et al. 2016).

Uneven performance of vanadium-doped  $\text{TiO}_2$  as photocatalyst has been reported. Some authors studied this kind of material as photocatalyst for the removal of diverse organic pollutants (Klosek and Raftery 2002; Wu and Chen 2004; Kamegawa et al. 2009; Ma et al. 2014; Belfaa et al. 2018; Sacco et al. 2019). On the other hand, in the case of 4-chlorophenol, previous studies revealed that a 1 nominal atomic percent doping level of vanadium in  $\text{TiO}_2$  reduced the photocatalytic degradation rates compared to the undoped one (Martin et al. 1994). Moreover, Plumejeau et al. (2016) reported that vanadium-doped  $\text{TiO}_2$  (1–10 mol%) exhibited very low activity for photocatalytic phenol degradation under UV irradiation, but they suggested that the tests had to be performed under visible light irradiation due to the E<sub>g</sub> shift to the visible range. Other authors also found that vanadium doping could shift the absorption edge of  $\text{TiO}_2$  to the visible light region (Khan et al. 2013). Despite the reported variability of V-doped  $\text{TiO}_2$  photoactivity, some authors suggested that significant improvements in doped  $\text{TiO}_2$  effectiveness are possible with a low concentration of dopant and the use of appropriate synthesis methods to limit lattice distortion (Hernández-Alonso et al. 2009).

The sol-gel method is widely used for doped  $\text{TiO}_2$  synthesis due to its versatility. Vanadium-doped materials synthesized with this method have shown good performance in the degradation of methylene blue (Iketani et al. 2004), crystal violet (Wu and Chen 2004), isobutanol (Kamegawa et al. 2009), and caffeine (Sacco et al. 2019). However, the synthesis conditions (V precursor, presence of water, type of acid, molar ratio between reactants, calcination temperature, etc.) were not deeply analyzed.

This paper aims to investigate the effect of using vanadyl acetylacetonate or ammonium metavanadate as vanadium precursors on the crystalline phase, surface area, surface species, optical property, and photocatalytic activity of V-doped  $\text{TiO}_2$  synthesized by sol-gel method. The synthesized materials were tested as photocatalysts for the degradation of phenol (the model compound) under UV and visible light irradiation in aqueous suspension. Its applicability was also extended to the degradation of other phenolic compounds (4-chlorophenol and 4-nitrophenol). Furthermore, the effect of the presence of Aldrich humic acid (as a model of NOM) was assayed to evaluate the selectivity of phenol degradation.

## Materials and methods

The materials were prepared by the sol-gel method. The procedure was adapted from Choi et al. (2010) using titanium (IV) isopropoxide ( $\text{Ti}(\text{C}_2\text{H}_6\text{O})_4$ , 97%, Aldrich, TTIP) as titanium precursor. Vanadyl acetylacetonate ( $\text{VO}(\text{acac})_2$ , 97%, Fluka) or ammonium metavanadate ( $\text{NH}_4\text{VO}_3$ , 99%, Sigma-Aldrich) were used as vanadium precursors, which in aqueous solution generated  $[\text{VO}(\text{H}_2\text{O})_5]^{2+}$  or  $[\text{VO}_2(\text{H}_2\text{O})_4]^+$ , respectively (Greenwood and Earnshaw 1997). In a typical synthesis, a solution A was prepared with 50 mL of absolute ethanol (Soria) and 5 mL of TTIP under a hood in a humidity-free atmosphere. Then, a solution B was prepared by dissolving the appropriate amount of vanadium precursor in 50 mL of distilled water with 110  $\mu\text{L}$  of  $\text{HNO}_3$  (65%, Anedra). Afterwards, solution A was added dropwise to solution B (1.8 mL per minute) under constant stirring (350 rpm). The molar ratio TTIP:EtOH: $\text{H}_2\text{O}$ : $\text{HNO}_3$  was 1:40:169:0.1. The suspension was aged by stirring for 24 h at 25 °C. The gel was dried at 100 °C for 24 h. The obtained crystals were ground and calcined at different temperatures, 400 °C, 500 °C, or 600 °C, for 1 h, with or without air circulation (constant supply of  $\text{O}_2$ ). The amount of vanadium precursors was chosen to give  $\text{TiO}_2$  material doping levels from 0.01 to 1.00 nominal atomic percent (at. %). A material without V addition was also prepared under the same experimental conditions as a reference. Synthesized materials and their preparation conditions are listed in Table 1.

To study the crystal structure patterns of the V-doped  $\text{TiO}_2$ , powder samples were examined by X-ray diffraction (XRD)

**Table 1** Synthesized materials and their preparation conditions

Material name	Vanadium precursor	Vanadium nominal content (at. %)	Calcination temperature (°C)
Ti-400	–	0.00	400
0.01VTi-400	VO(acac) <sub>2</sub>	0.01	400
0.01VTi-500	VO(acac) <sub>2</sub>	0.01	500
0.01VTi-600	VO(acac) <sub>2</sub>	0.01	600
0.05VTi-400(ac)	VO(acac) <sub>2</sub>	0.05	400 with air circulation
0.05VTi-400	VO(acac) <sub>2</sub>	0.05	400
0.05V <sub>M</sub> Ti-400(ac)	NH <sub>4</sub> VO <sub>3</sub>	0.05	400 with air circulation
0.05V <sub>M</sub> Ti-400	NH <sub>4</sub> VO <sub>3</sub>	0.05	400
0.10VTi-400	VO(acac) <sub>2</sub>	0.10	400
1.00VTi-400(ac)	VO(acac) <sub>2</sub>	1.00	400 with air circulation
1.00VTi-400	VO(acac) <sub>2</sub>	1.00	400
1.00V <sub>M</sub> Ti-400(ac)	NH <sub>4</sub> VO <sub>3</sub>	1.00	400 with air circulation
1.00V <sub>M</sub> Ti-400	NH <sub>4</sub> VO <sub>3</sub>	1.00	400

using a Philips diffractometer PW-1390 with Cu K $\alpha$  radiation. The Raman scattering measurements were performed in the backscattering geometry at room temperature in air, using a Jobin-Yvon T64000 triple spectrometer (with a confocal microscope and a N<sub>2</sub>-cooled charge-coupled device detector, and excited by a 514.5 nm line of argon laser with an output power of less than 5 mW). Micromeritics ASAP 2020 was used to determine the Brunauer-Emmett-Teller (BET) surface areas using N<sub>2</sub> as the adsorptive gas. UV-Vis diffuse reflectance spectra (DRS) were obtained using a UV-Vis Perkin-Elmer Lambda 35 spectrophotometer. The H<sub>2</sub>-temperature programmed reduction (H<sub>2</sub>-TPR) experiments were performed on Quantachrome Jr. Instrument fitted with a thermal conductivity detector.

X-ray photoelectron spectroscopy (XPS) measurements and analyses were performed in a PHI 548 spectrometer with a double-pass cylindrical mirror analyzer, using Al K $\alpha$  nonmonochromatic radiation (300 W and 20 mA). The resolution spectra were taken at 50 eV pass energy (absolute resolution of about  $\pm 0.5$  eV). The operation base pressure was  $5 \times 10^{-9}$  Torr. The C 1s binding energy was taken as a charge reference and fixed at 285.0 eV. The signal deconvolution was performed using Shirley-type background subtraction and sum of Gaussian-Lorentzian functions. The atomic ratios were estimated by relating the peak areas after the background subtraction and corrected relative to the corresponding atomic sensitivity factors to an approximate absolute error of 20%.

Phenol, 4-nitrophenol, and 4-chlorophenol degradation was studied. The reaction mixtures were prepared by ultrasonically dispersing 1 g L<sup>-1</sup> of the catalyst in 50, 100, or 250  $\mu$ M aqueous solution of the phenolic compound. For the selectivity assay, Aldrich humic acid (AHA) was used as model of natural organic matter. The initial amount of AHA was 12 mg L<sup>-1</sup> because it is the average concentration

usually reported for natural waters (Beck et al. 2012). All experiments were performed at the inherent pH of the mixture (around 6).

Rayonet photochemical reactor RPR-100 (Southern New England Ultraviolet Company) with ultraviolet (UV) or visible (VIS) lamps was used. The lamp spectra were determined in a previous work, showing emission maxima of UV and VIS lamps at 365 and 577 nm, respectively (Martin et al. 2017). Sampling was performed periodically. Phenol concentrations in the filtered samples were determined using HPLC (C18 column, Restek Pinnacle II, particle size: 5  $\mu$ m, id: 2.1 mm, length: 250 mm) and a 50/50 (v/v) methanol/H<sub>3</sub>PO<sub>4</sub> (0.2%) mixture as eluent at 0.1 mL min<sup>-1</sup> constant flux.

For the experiment in the presence of AHA, the total organic carbon (TOC) was determined by a high-temperature carbon analyzer model TOC 5000A from Shimadzu. The detection limit was 1 ppm C. This measurement was carried out for a more effective evaluation of the degree of mineralization reached by all organic compounds in the mixture (phenol, AHA, and all possible reaction intermediates).

To evaluate vanadium leaching from the catalysts, metal ion concentrations were determined using ICP-mass spectrometry (ICP-MS, NexION 300X, Perkin-Elmer Co.). Sampling was carried out at the end of the irradiation period, and the samples were filtered through a cellulose membrane (pore size, 0.45  $\mu$ m).

Phenol concentration evolution in aqueous solution, with irradiation (without catalyst) and without irradiation (with each catalyst), was analyzed to test the direct photolysis and adsorption of phenols on the materials, respectively. It should be noted that in all these control assays, the percentage of degradation or adsorption of phenols was less than 15%.

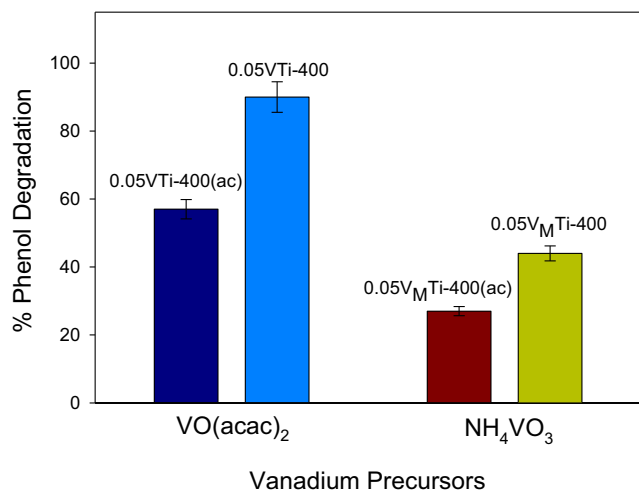


**Fig. 1** Effect of vanadium precursors and calcination conditions on the efficiency of phenol degradation ([Phenol]<sub>0</sub> = 50 μM, UV lamps, 3 h, 1 g L<sup>-1</sup> of catalyst) using materials with 0.05 at. % of V and calcined at 400 °C. *ac* air circulation

## Results and discussion

### Effect of synthesis conditions on phenol degradation efficiency

Materials containing 0.05 at. % of V were prepared using two different vanadium precursors (VO(acac)<sub>2</sub> and NH<sub>4</sub>VO<sub>3</sub>) and were calcined at 400 °C, with or without air circulation. Their efficiency as photocatalysts for the degradation of phenol (50 μM, 3 h, UV lamps) was evaluated. The results are shown in Fig. 1. The activity of the materials synthesized using VO(acac)<sub>2</sub> was higher than that using NH<sub>4</sub>VO<sub>3</sub>. Moreover, calcination without air circulation improved the photoactivity (with both precursors).

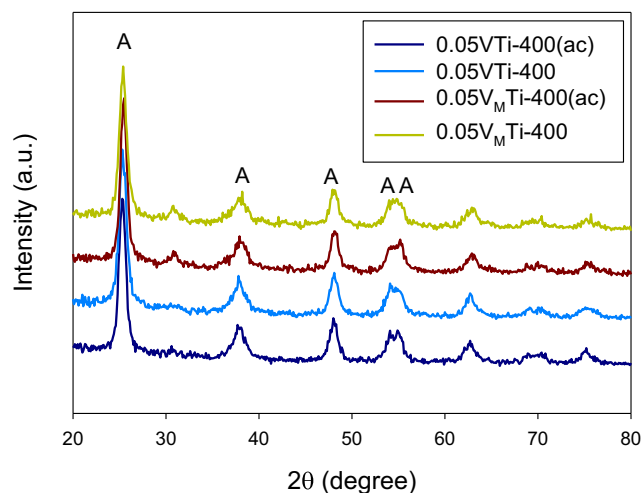


**Fig. 2** Effect of vanadium precursors and calcination conditions on XRD patterns of materials synthesized with 0.05 at. % of V and calcined at 400 °C. *ac* air circulation, A anatase

**Table 2** Structural and textural properties of photocatalysts synthesized with two different vanadium precursors

Photocatalyst	Anatase crystallite size (nm)	S <sub>BET</sub> (m <sup>2</sup> g <sup>-1</sup> )	V <sub>p</sub> (cm <sup>3</sup> g <sup>-1</sup> )	D <sub>p</sub> (nm)
0.05VTi-400(ac)	12.2	100	0.13	3.6
0.05VTi-400	11.8	91	0.15	4.5
0.05V <sub>M</sub> Ti-400(ac)	13.2	57	0.10	4.6
0.05V <sub>M</sub> Ti-400	12.4	78	0.13	4.6

XRD patterns of the synthesized catalysts were recorded. For these catalysts, the anatase phase of TiO<sub>2</sub> was the main one (Fig. 2). This crystalline phase was identified by comparison with the International Center for Diffraction Data (ICDD), JCPDS ID No. 89–4921. The crystal size value was estimated from the peak broadening due to the reflection of (101) plane by Scherrer equation (Klug and Alexander 1974). In all cases, the crystal size values were similar, averaging 12.4 ± 0.6 nm, without differences due to precursors or calcination conditions (see Table 2).

Nitrogen adsorption–desorption isotherms of the prepared photocatalyst samples were tested to evaluate the textural properties (Fig. 3). All the isotherms exhibited typical type IV behavior with a hysteresis loop caused by capillary condensations within the mesopores, according to Brunauer–Deming–Deming–Teller (BDDT) classification (Sing et al. 1985). The average pore diameters (D<sub>p</sub>) obtained from BJH desorption, volume adsorption (V<sub>p</sub>), and specific surface area (S<sub>BET</sub>) values are listed in Table 2. Materials synthesized using VO(acac)<sub>2</sub> presented higher specific surface areas than those prepared using NH<sub>4</sub>VO<sub>3</sub>. The increment in surface area value supported the observed improvement in photoreactivity (see Fig. 1).

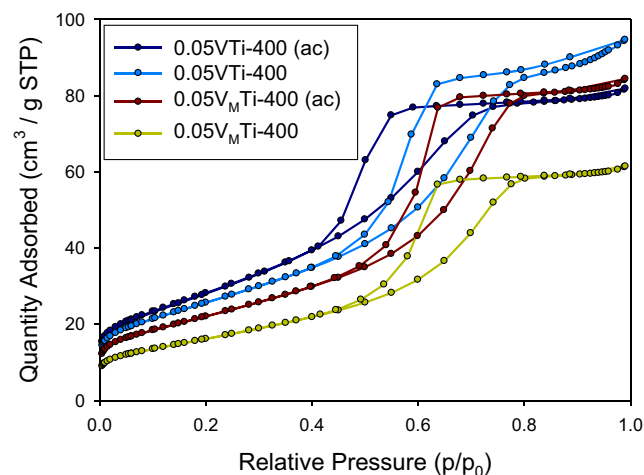


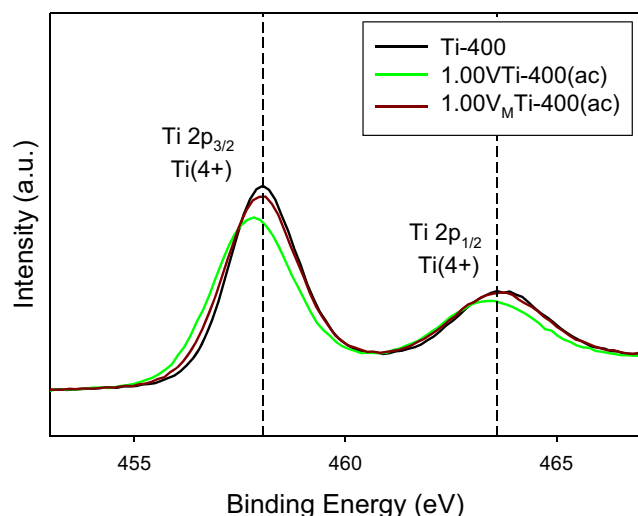
**Fig. 3** Effect of vanadium precursors and calcination conditions on N<sub>2</sub> sorption isotherms at 77 K of materials synthesized with 0.05 at. % of V and calcined at 400 °C. *ac* air circulation

XPS studies were performed to analyze the surface species of the catalysts. Unfortunately, the amount of V present in these catalysts (0.05 at. %) did not allow a proper determination with the available equipment. Then, a series of materials with 1.00 at. % of V (similar synthesis conditions) was prepared (see Table 1). Figure 4 shows the Ti 2p XPS peak regions for Ti-400, 1.00VTi-400(ac), and 1.00V<sub>M</sub>Ti-400(ac).

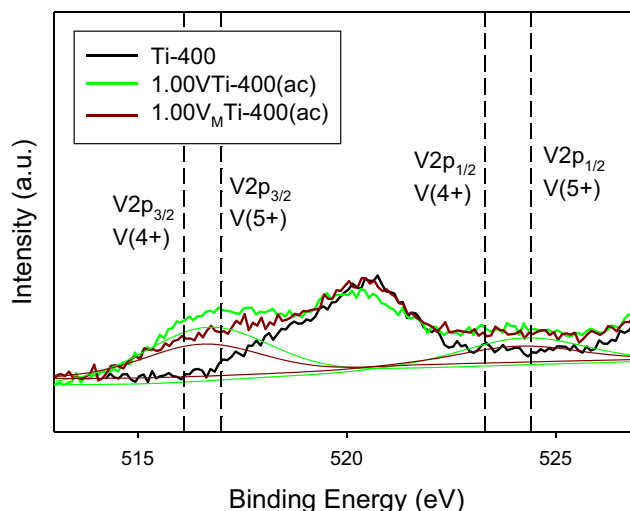
For Ti-400 and 1.00V<sub>M</sub>Ti-400(ac), peaks at 458.0 and 463.6 eV, corresponding to Ti 2p<sub>3/2</sub> and Ti 2p<sub>1/2</sub>, were observed. These values could be assigned to the Ti(4+) oxidation state in TiO<sub>2</sub>. A slight shift in the binding energies was detected in the spectra of 1.00VTi-400(ac). Due to the values reported for Ti(3+), 457.55, and 463.30 eV (Chen et al. 2017), these shifts could suggest that the titanium was in both oxidation states (O–Ti<sup>4+</sup>–O and O–Ti<sup>3+</sup>–O bonds). A similar behavior was reported by Chen and coworkers for TiO<sub>2</sub> doped with 0.02 to 0.4 at. % V (Chen et al. 2017). Moreover, the change of Ti 2p<sub>3/2</sub> peak with respect to that of pure TiO<sub>2</sub> could indicate that the V ion was incorporated into the TiO<sub>2</sub> lattice and led to Ti<sub>2</sub>O<sub>3</sub> formation accompanied by oxygen defects (Ma et al. 2014).

Figure 5 shows the V 2p XPS peak regions for Ti-400, 1.00VTi-400(ac), and 1.00V<sub>M</sub>Ti-400(ac) surfaces.

Broadening of the spectra could be observed at around 516 and 523 eV for 1.00VTi-400(ac) and 1.00V<sub>M</sub>Ti-400(ac). These regions were assigned to V2p<sub>3/2</sub> and V2p<sub>1/2</sub>. Colton and coworkers (Colton et al. 1978) reported values of 515.5, 516.1, and 517.0 eV for V(3+), V(4+), and V(5+), respectively. The estimated values from deconvolution of the signals suggested that the main species was V(4+), with small amounts of V(5+). A 1.3 ± 0.3 and 0.7 ± 0.1 at. % of V content at the surface could be estimated for 1.00VTi-400(ac) and 1.00V<sub>M</sub>Ti-400(ac), respectively. The higher amount of V on 1.00VTi-400(ac) accounted for the higher efficiency of this



**Fig. 4** XPS of Ti-400, 1.00VTi-400(ac), and 1.00V<sub>M</sub>Ti-400(ac) showing Ti 2p spectra



**Fig. 5** XPS of Ti-400, 1.00VTi-400(ac), and 1.00V<sub>M</sub>Ti-400(ac) showing V 2p spectra and deconvolution of the signals of 1.00VTi-400(ac) and 1.00V<sub>M</sub>Ti-400(ac)

material with respect to 1.00V<sub>M</sub>Ti-400(ac). A more detailed analysis of the spectra could not be done due to the overlap of the signals from O 1s and V 2p and the small amount of V on the materials.

Although the best performance obtained with materials prepared from VO(acac)<sub>2</sub> could be explained by their greater surface area and a higher surface content of V, no correlation of these parameters with calcination conditions was observed.

When the material was calcined without air circulation, its efficiency as a photocatalyst for the degradation of phenol increased (see Fig. 1). This behavior may be explained considering that an oxidizing atmosphere such as air stimulates the formation of the highest oxidation state (+5) of the vanadium present in the material.

H<sub>2</sub>-TPR experiments were performed to study oxidation states of vanadium associated with the calcination conditions, 400 °C with or without air circulation. For a proper determination using the available equipment, materials with 1.00 at. % of V were studied. Figure 6 shows the H<sub>2</sub>-TPR profiles of 1.00VTi materials calcined at 400 °C with or without air circulation in comparison with undoped TiO<sub>2</sub> (Ti-400).

According to Ghampson et al. (2017), the profile of a commercial TiO<sub>2</sub> presents a broad reduction peak with a maximum at 508 °C, which originates from the surface reduction of TiO<sub>2</sub>. In our case, this broad peak is almost imperceptible, with a maximum at around 550 °C (see Ti-400 in Fig. 6).

The H<sub>2</sub>-TPR profiles of V-doped TiO<sub>2</sub> presented a main reduction peak with a maximum at 454 and 458 °C for 1.00VTi-400 and 1.00VTi-400(ac), respectively. Moreover, we could detect the presence of another peak at a lower temperature (around 250 °C) for the catalyst calcined with air circulation (see 1.00VTi-400(ac) in Fig. 6).

The reduction profiles could be considered interferences of different reduction steps of vanadium, V(5+) → V(4+) →

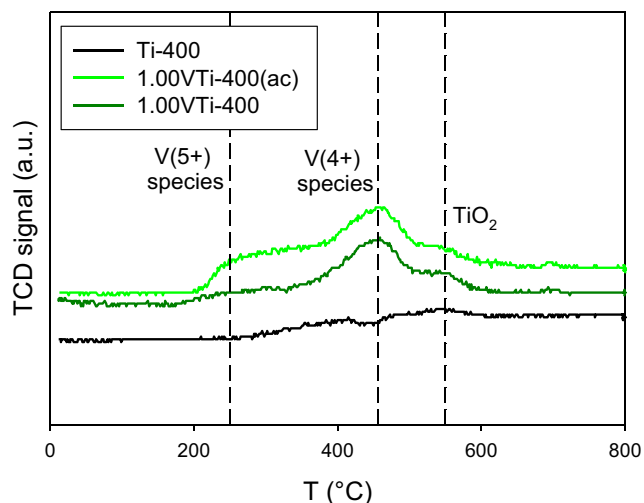


**Fig. 6** H<sub>2</sub>-TPR profiles of the catalysts (0.1 g catalyst; flow rate, 20 mL min<sup>-1</sup>; 10% H<sub>2</sub>/N<sub>2</sub>; heating rate, 10 °C min<sup>-1</sup>)

V(3+), and of different VO<sub>x</sub> species (Machold et al. 2008). The hydrogen consumption peaks of V<sub>2</sub>O<sub>5</sub> comprised three peaks at 604 °C, 632 °C, and 749 °C; these temperatures corresponded to the reduction of V<sub>2</sub>O<sub>5</sub> → V<sub>6</sub>O<sub>13</sub>, V<sub>6</sub>O<sub>13</sub> → V<sub>2</sub>O<sub>4</sub>, V<sub>2</sub>O<sub>4</sub> → V<sub>2</sub>O<sub>3</sub>, respectively. These peaks shifted to a lower temperature after loading V on TiO<sub>2</sub>, indicating the strong interaction between V and Ti species (He et al. 2017). VO<sub>x</sub> species with different degree of polymerization could coexist on the surface of TiO<sub>2</sub>: isolated species are more easily reduced than polymeric species, and these, in turn, are faster than crystalline species because of V interaction with TiO<sub>2</sub> (Chang et al. 2012; Gallastegi-Villa et al. 2015; Hidalgo et al. 2016). Bulushev et al. (2002) observed three types of surface vanadia species on vanadia/titania catalysts with the following maximum peak temperatures: isolated monomeric species (≤ 497–507 °C), polymeric species (537 °C), and bulk amorphous V<sub>2</sub>O<sub>5</sub> (573 °C). Afterwards, we could detect the presence of VO<sub>x</sub> species, predominantly of monomeric character, along with evidence of more easily reducible V(5+) species for the catalyst treated with airstream, 1.00VTi-400 (ac).

Assuming that the materials with lower V contents (0.05 at. %) could present a similar behavior, the preponderance of V(4+) could explain their higher performance as photocatalyst. This result is in agreement with Iketani et al. (2004), who attributed the decrease in photoactivity of doped TiO<sub>2</sub> to the presence of vanadium in the highest oxidation state (5+). Moreover, Choi et al. (Choi et al. 1994) argued that the photoactivity of V(5+) is significantly lower than that of V(4+) in TiO<sub>2</sub>, since V(5+) can only trap electrons, while V(4+) can act as both an electron trap and a hole trap.

Among the studied materials, the best photocatalyst was 0.05VTi-400, reaching 90% phenol degradation ([phenol]<sub>0</sub> = 50 μM) in 3 h of irradiation with UV lamps. Based on this

result, the influence of the catalyst vanadium contents (prepared using VO(acac)<sub>2</sub> and calcined at 400 °C without air circulation) on its photoactivity was studied. The results are presented in Fig. 7. The optimum content of V was 0.01 at. %, since 0.01VTi-400 showed 100% phenol degradation in 3 h of irradiation with UV lamps. The existence of an optimum metal doping level is a behavior widely observed in similar materials (Jaiswal et al. 2012).

One of the main drawbacks of heterogeneous catalysts is the leaching of the active phase into the liquid phase. Then, the concentrations of vanadium after using each catalyst were determined in the reaction mixture. For all the materials (0.01VTi-400, 0.05VTi-400, 0.1 VTi-400, and 1.00VTi-400), the values were around 0.5 ppb, below the recommended limit value (15 ppb) (Princeton University 2016). The Ti values in solution were below the detection limit (i.e., less than 5 ppb). As far as we know, there are no values to regulate the presence of titanium species in aqueous solution.

X-ray diffraction patterns of doped TiO<sub>2</sub> with different V content exhibited characteristic peaks of the anatase phase, indicating that this phase is the principal one (data not shown here). No evidence of peaks that could be assigned to crystalline phases of V (according to JCPDS No. 81-2392 and 89-2482 for VO<sub>2</sub> and V<sub>2</sub>O<sub>5</sub>, respectively) was found. This suggested that the doping level employed did not lead to the formation of discrete phases of vanadium, and the metal ion could have joined the network of TiO<sub>2</sub>. It could also be that vanadium species formed during synthesis were well dispersed on the TiO<sub>2</sub> surface or too small to be detected by the equipment used (Yu et al. 2019). In all cases, the anatase crystal size values were similar, averaging 14 ± 1 nm. XRD results revealed no structural differences among samples, since no peaks arising from vanadium species were detected.

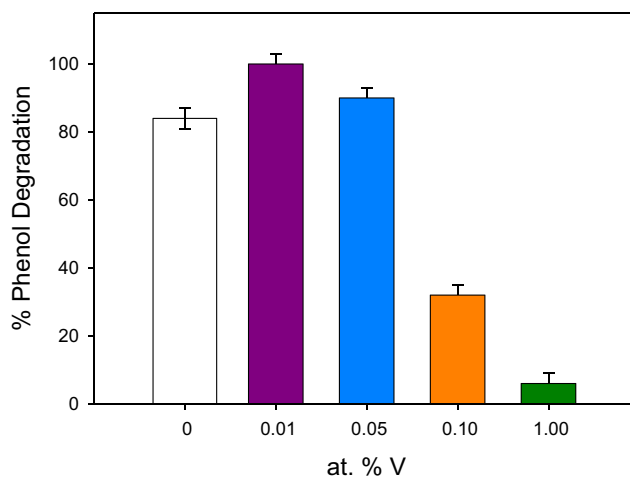


**Fig. 7** Effect of vanadium content on the efficiency of phenol degradation ([phenol]<sub>0</sub> = 50 μM, UV lamps, 3 h, 1 g L<sup>-1</sup> of catalyst). All the materials were prepared using VO(acac)<sub>2</sub> and calcined at 400 °C without air circulation

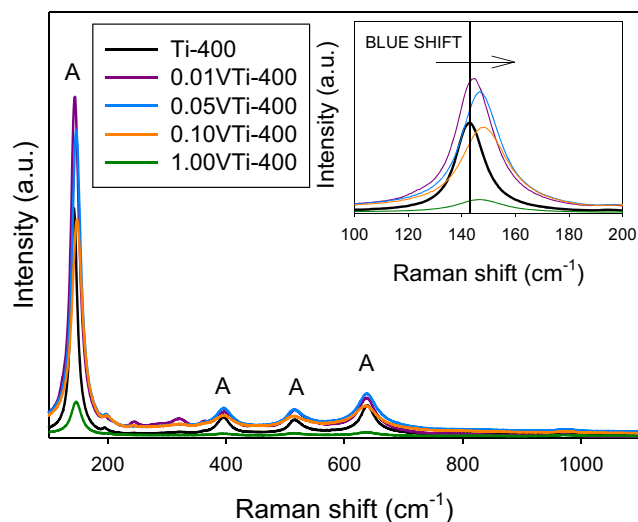


**Fig. 8** Effect of vanadium content on Raman spectra of undoped and vanadium-doped catalysts using  $\text{VO}(\text{acac})_2$  as V precursor and calcined at 400 °C without air circulation. The inset is the magnified Raman pattern from 100 to 200  $\text{cm}^{-1}$

Since Raman spectroscopy is known to be a rather sensitive tool to study the microstructure of nanosized materials (Khodakov et al. 1999; Reddy et al. 2009; Oh and Shin 2013; Loan and Long 2019), Raman spectra of undoped and vanadium-doped samples were taken. At first, the Raman spectra (Fig. 8) confirmed the presence of anatase as the main phase for all the catalysts (Zhang et al. 2006; Anju et al. 2018; Loan and Long 2019). A blue shift of the main peak, at 143  $\text{cm}^{-1}$ , for the Eg Raman mode of anatase corresponding to the symmetric stretching vibration of O-Ti-O bond, can be clearly seen for the doped materials in the inset of Fig. 8. Yu and coworkers reported that this blue shift could be attributed to structural changes, such as oxygen vacancies and various defects or the formation of Ti(3+) centers, as a result of V doping (Yu et al. 2019). It can be considered that V ions were doped in the  $\text{TiO}_2$  lattice.

Textural properties of doped  $\text{TiO}_2$  were determined by  $\text{N}_2$  adsorption–desorption isotherms. All the isotherms, Fig. 9, exhibited typical type IV behavior (Sing et al. 1985). Table 3 shows the obtained values of  $D_p$  (BJH desorption),  $V_p$  (BJH desorption), and  $S_{\text{BET}}$ . No appreciable changes were

**Table 3** Textural and optical properties of photocatalysts synthesized with different levels of vanadium doping

Photocatalyst	$S_{\text{BET}}$ ( $\text{m}^2 \text{g}^{-1}$ )	$V_p$ ( $\text{cm}^3 \text{g}^{-1}$ )	$D_p$ (nm)	E <sub>bg</sub> (eV)
Ti-400	84	0.11	3.8	3.04
0.01VTi-400	96	0.17	4.8	3.02
0.05VTi-400	91	0.15	4.5	2.97
0.10VTi-400	72	0.13	5.1	2.86
1.00VTi-400	81	0.10	3.6	2.63

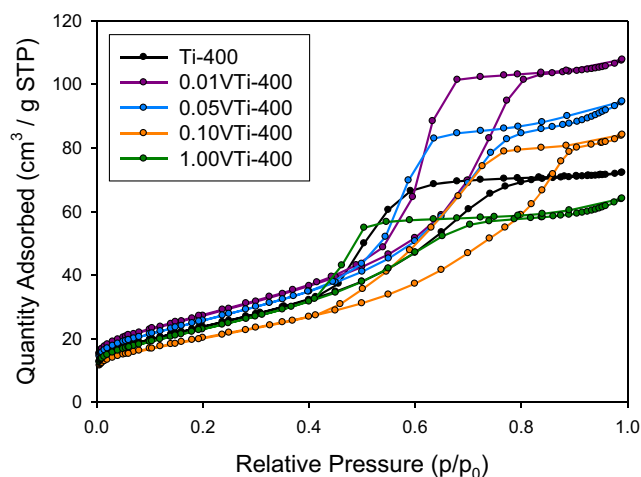


**Fig. 9** Effect of vanadium content on nitrogen sorption isotherms at 77 K. All the materials were prepared using  $\text{VO}(\text{acac})_2$  and calcined at 400 °C without air circulation

observed for the doped materials. However, the  $S_{\text{BET}}$  value for 0.01VTi-400 was the highest of the group.

The DRS spectra of undoped and V-doped  $\text{TiO}_2$  samples were performed (Fig. 10). Compared with the spectrum of undoped  $\text{TiO}_2$ , a red shift appeared in the series of V-doped  $\text{TiO}_2$  catalysts. In addition, its extension depended on the amount of vanadium doping, and the higher the load of vanadium, the greater the red shift. The E<sub>bg</sub> of all samples was estimated from the following equation (Ma et al. 2014):

$$\alpha \times h\nu = C \times (h\nu - E_{\text{bg}})^n$$

where  $\alpha$  is the linear absorption coefficient of the material,  $C$  is the model adjustment constant,  $h\nu$  is the photon energy (eV), and  $n$  is the constant type of optical transition, with a value of  $n = 1/2$  for permitted direct transitions ( $\text{TiO}_2$ ). The

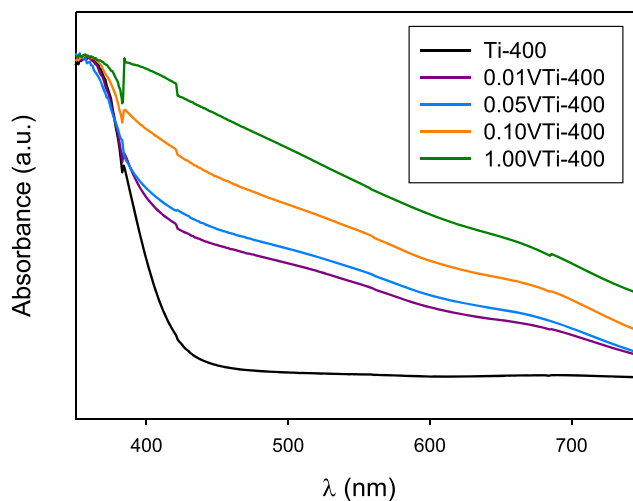


**Fig. 10** Effect of vanadium content on UV-Vis diffuse reflectance spectra (DRS). All the materials were prepared using  $\text{VO}(\text{acac})_2$  and calcined at 400 °C without air circulation

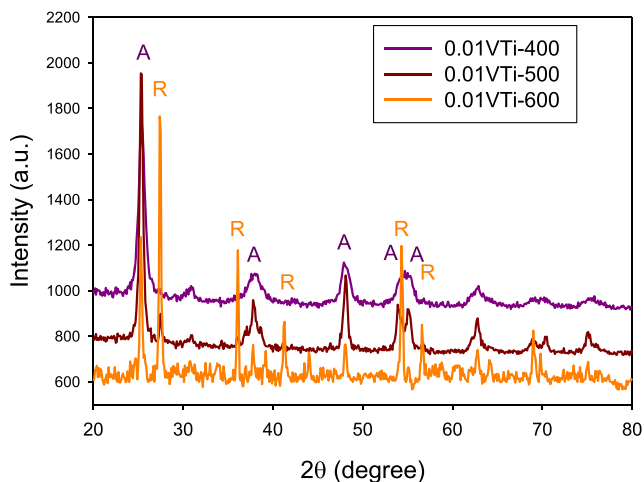


**Fig. 11** XRD for materials with the optimum content of V, calcined at different temperatures (400, 500, and 600 °C) without air circulation. A anatase, R rutile

estimated values (Table 3) showed the narrowing of E<sub>g</sub> with the V content. The absorption edge shift of V-doped TiO<sub>2</sub> was reported by many authors (Liu et al. 2009; Jaiswal et al. 2012; Ren et al. 2015). The incorporation of V(4+) into the TiO<sub>2</sub> lattice induced some new states near the edge of the valence and conduction bands, respectively, causing the observed behavior (Ren et al. 2015).

Materials with the optimum content of V (0.01 at. %) and calcined at different temperatures (400, 500, and 600 °C) were tested. An increase in the calcination temperature resulted in a significant improvement in the crystallinity of the material and a mixed anatase-rutile phase (Fig. 11). Additionally, a drastic reduction of the S<sub>BET</sub> values was determined from N<sub>2</sub> physisorption isotherms (Fig. 12 and Table 4). Moreover, the increment in calcination temperature did not improve their efficiency as photocatalysts, as expected from the presence of rutile phase (less photoactive than anatase phase) and the

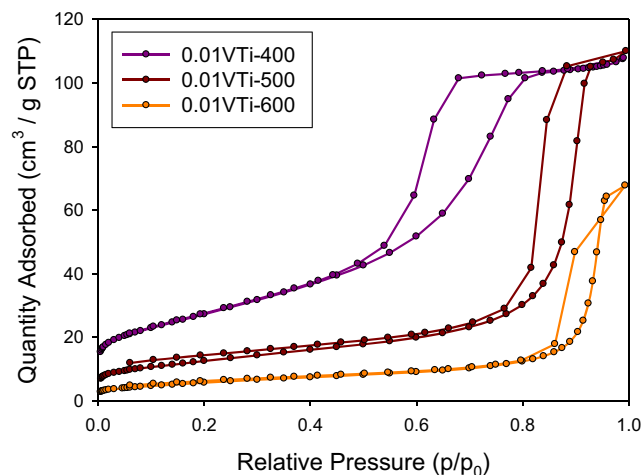


**Fig. 12** Nitrogen sorption isotherms at 77 K of materials synthesized with 0.01 at. % of V calcined at different temperatures (400, 500, and 600 °C) without air circulation

**Table 4** Textural properties of 0.01VTi photocatalysts calcined at different temperatures

Photocatalyst	S <sub>BET</sub> (m <sup>2</sup> g <sup>-1</sup> )	V <sub>p</sub> (cm <sup>3</sup> g <sup>-1</sup> )	D <sub>p</sub> (nm)
0.01VTi-400	96	0.17	4.8
0.01VTi-500	44	0.17	12.0
0.01VTi-600	20	0.10	16.9

reduction of the S<sub>BET</sub> values. Similar results were reported by Ren et al. (2015) when studying the effect of calcination temperature on the photocatalytic oxidation rate of propylene over 1% V-TiO<sub>2</sub> (nanotubes). They observed a high photocatalytic activity at 500 °C, but as the calcination temperature increased, the photocatalytic activity decreased rapidly and was completely lost at 800 °C.

### Study of the operating conditions for the degradation of phenols

The 0.01VTi-400 catalyst was the most effective, so it was tested under different experimental conditions. Phenol degradation was studied by varying the initial concentration of this compound (50, 100, and 250 μM). For assays using UV lamps, the degradation percentage was around 96 ± 4% in all cases, as shown in Fig. 13.

Furthermore, when using VIS lamps, phenol degradation showed markedly lower values, as expected from the light absorption of the material. For the lowest initial phenol

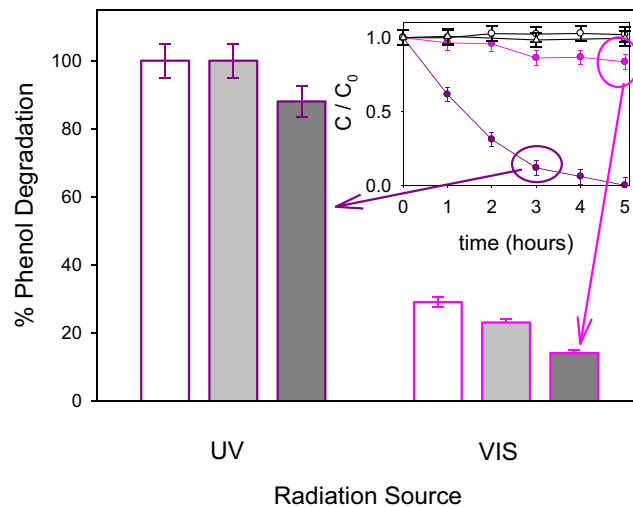


**Fig. 13** Effect of initial phenol concentration on the percentage of degradation with 0.01VTi-400 (1 g L<sup>-1</sup>) after 3 h of irradiation with UV lamp or after 5 h of irradiation with VIS lamps. White, gray, and black bars indicate initial phenol concentrations of 50, 100, and 250 μM, respectively. Inset: Time evolution of phenol concentration ([phenol]<sub>0</sub> = 250 μM) with UV lamp (purple) or with VIS lamps (pink). Direct photolysis (white circles) and adsorption (white triangles) were included as control assays

concentration (50  $\mu\text{M}$ ), a maximum of 30% degradation was attained. It is noteworthy that although it is a low value, it should not be ruled out because of its potential use in larger scale systems, where the use of sunlight has a favorable impact on the costs associated with the treatment.

For pure  $\text{TiO}_2$  excited by UV irradiation,  $\text{HO}^\cdot$  radicals are the primary oxidation species responsible for phenol degradation and/or mineralization: hydroquinone and catechol are the main intermediates from this attack (Martin et al. 2015). In the case of metal-doped  $\text{TiO}_2$ , both  $\text{HO}^\cdot$  radicals and direct oxidation could be employed (Grabowska et al. 2012). However, no significant adsorption of phenol on the V-doped catalysts was observed, making the contribution of direct oxidation less important in our studies. Further work on this line of investigation is currently being performed.

The reactivity of aromatic compounds, including phenols, can be drastically affected by the electronic nature of the substituent groups. The  $\text{HO}^\cdot$  radical is a strong electrophile, with high affinity for the electron-rich sites of aromatic compounds. In the case of p-substituted phenols, the  $\text{HO}^\cdot$  radical reacts with the more negatively charged unsubstituted positions. The Hammett constant represents the effect of various substituent groups on the electronic character of a given aromatic system. Hammett constant values are numbers that sum up the total electrical effects of a group attached to a certain aromatic system. A positive value of  $\sigma$  indicates an electron-withdrawing group and a negative value, an electron-donating group (McDaniel and Brown 1957). Although Hammett correlations are primarily used for reactions occurring in homogeneous solutions, they have also been successfully applied to heterogeneous systems (O'Shea and Cardona 1994; Tolosana-Moranchel et al. 2019).

To evaluate the applicability of 0.01VTi-400 to other contaminants, experiments were performed using phenol, 4-chlorophenol, or 4-nitrophenol under the same experimental conditions (initial concentration 50  $\mu\text{M}$ , irradiation with UV lamps for 3 h, continuous stirring). The Hammett constant values for these chosen substituents were 0.227 (for “—Cl”) and 0.778 (for “—NO<sub>2</sub>”), both electron-withdrawing groups but with very different strength (McDaniel and Brown 1957).

The evolution of substituted phenol concentrations in aqueous solution with irradiation (UV lamps), without catalyst, was studied to quantify the photolysis of each compound. A decrease in concentration of 2%, 15%, and 12% was observed for phenol, 4-chlorophenol, and 4-nitrophenol. That is, the presence of a second substituent in the benzene ring of the compound promoted photolysis. Furthermore, the adsorption of compounds on 0.01VTi-400 was studied by monitoring their concentration in the presence of the catalyst, without irradiation. In these assays, a similar decrease of concentration was found for the three compounds ( $10 \pm 3\%$ ).

Time evolution curves of the concentration of the three phenolic compounds are shown in Fig. 14. The degradation

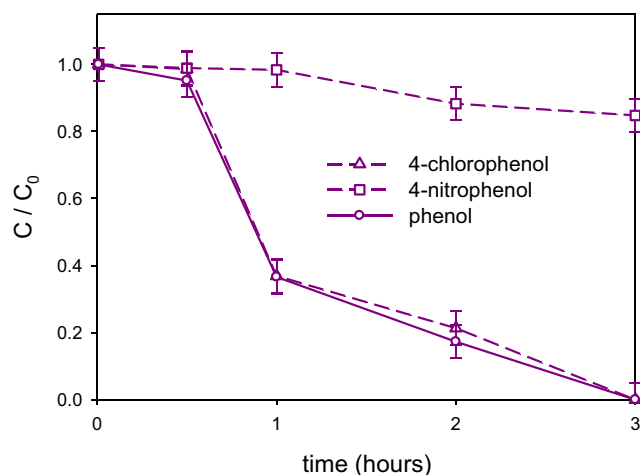


**Fig. 14** Time evolution of phenol (circles), 4-chlorophenol (triangles), or 4-nitrophenol (squares) using 0.01VTi-400 (1 g L<sup>-1</sup>) after 3 h of irradiation with UV lamp (initial concentration, 50  $\mu\text{M}$ )

of 4-chlorophenol was the same as that of phenol (100% at 3 h), indicating that the presence of the chloride group “—Cl” did not change the reactivity of phenol. However, the abatement of 4-nitrophenol was very low (15% at 3 h), showing a strong deactivating effect of the nitro group “—NO<sub>2</sub>”. Moreover, this 15% decrease could be assigned to direct photolysis of the compound without photocatalytic degradation.

These studies showed that the photocatalyst 0.01VTi-400 is appropriate to degrade substituted phenols, except for those that have a strong deactivating group for electrophilic attack (such as the nitro group).

Selective oxidation of certain pollutants has been a major challenge in photocatalysis, since normal source water contains low concentrations of toxic substances along with high concentrations of natural organic matter. The selectivity of 0.01VTi-400 for phenol degradation ( $[\text{phenol}]_0 = 50 \mu\text{M}$ ) in the presence of AHA was tested using UV lamps (for 3 h). Phenol degradation was lower than in the corresponding experiment without AHA, showing the inhibition effect of AHA (Palacio et al. 2017). It could be assumed that AHA acts as radical scavenger because some electron-rich moieties (e.g., phenolic groups) in its molecular structure are readily attacked by  $\text{HO}^\cdot$  (Deng et al. 2017). However, the observed percentage (68%) is high enough to consider 0.01VTi-400 as a promising material for natural water applications. Moreover, mineralization reached 49% (by TOC determinations), indicating the low formation of persistent intermediates. Further work on this line of investigation is currently being performed.

## Conclusion

The materials prepared from  $\text{VO}(\text{acac})_2$  presented higher photocatalytic activity than those prepared from  $\text{NH}_4\text{VO}_3$ , which could be related to the increase in the surface area values and

in the relative amounts of incorporated V. Calcination with air circulation promoted the highest oxidation state of vanadium, decreasing the photoactivity of the materials.

The optimum content of vanadium found under the study conditions was 0.01 nominal atomic %. No improvement in phenol degradation efficiency was observed when the calcination temperature of the material was increased between 400 and 600 °C.

The best photocatalyst (0.01VTi-400) was able to achieve the complete degradation of phenol (50 µM) in 3 h of irradiation with UV lamps and 30% degradation of phenol (50 µM) in 5 h of irradiation with VIS lamps. Moreover, despite the presence of Aldrich humic acid in the reaction mixture, the degradation of phenol (with UV lamps) reached 68%.

Additionally, as indicated by tests with 4-chlorophenol and 4-nitrophenol, the photocatalyst 0.01VTi-400 can be applied to the degradation of phenolic compounds when the substituent is an activating or a weak inactivating group (for electrophilic reactions).

The performance of 0.01VTi-400 points out its potential use in further applications.

**Acknowledgments** JAR and PIV are research members of CONICET. MP is a CPA member of CONICET. LR thanks CONICET for a doctoral studentship and SACAT for the internship under Dr. Miguel De Sanchez supervision. The authors wish to thank Pablo Fetsis and Juan Tara for their TPR and sorptometry experimental contribution.

**Authors' contributions** LR: Investigation, visualization, writing - original draft, and writing - review and editing. MP: Investigation. PIV: Conceptualization, resources, writing - original draft, writing - review and editing, supervision, project administration, and funding acquisition. JAR: Conceptualization, resources, writing - original draft, writing - review and editing, supervision, project administration, and funding acquisition.

**Funding** This study was funded by Grants X835 from Universidad Nacional de La Plata and PIP 2015 0329 from Consejo Nacional de Investigaciones Científicas y Técnicas de la República Argentina.

**Data availability** All data generated or analyzed during this study are included in this published article.

## Compliance with ethical standards

**Competing interests** The authors declare that they have no competing interests.

**Ethics approval and consent to participate** Not applicable.

**Consent for publication** Not applicable.

## References

Anju KR, Thankapan R, Rajabathar JR, Al-Lohedan HA (2018) Hydrothermal synthesis of nanosized (Fe, Co, Ni)-TiO<sub>2</sub> for

- enhanced visible light photosensitive applications. *Optik (Stuttg)* 165:408–415. <https://doi.org/10.1016/j.ijleo.2018.03.091>
- Beck M, Dellwig O, Fischer S, Schnetger B, Brumsack HJ (2012) Trace metal geochemistry of organic carbon-rich watercourses draining the NW German coast. *Estuar Coast Shelf Sci* 104:66–79. <https://doi.org/10.1016/j.ecss.2012.03.025>
- Belfaa K, Lassoued MS, Ammar S et al (2018) Synthesis and characterization of V-doped TiO<sub>2</sub> nanoparticles through polyol method with enhanced photocatalytic activities. *J Mater Sci: Mater Electron* 29: 10269–10276. <https://doi.org/10.1007/s10854-018-9080-6>
- Bulushev DA, Kiwi-Minsker L, Rainone F, Renken A (2002) Characterization of surface vanadia forms on V/Ti-oxide catalyst via temperature-programmed reduction in hydrogen and spectroscopic methods. *J Catal* 205:115–122. <https://doi.org/10.1006/jcat.2001.3427>
- Cai J, Zhou M, Du X, Xu X (2021) Enhanced mechanism of 2,4-dichlorophenoxyacetic acid degradation by electrochemical activation of persulfate on blue-TiO<sub>2</sub> nanotubes anode. *Sep Purif Technol* 254:117560. <https://doi.org/10.1016/j.seppur.2020.117560>
- Chang HY, Wang SP, Chang JR, Sheu HS, Shyu SG (2012) Synchrotron radiation PXRD investigation of V<sub>2</sub>O<sub>5</sub>/TiO<sub>2</sub> catalysts for 1,2-dichlorobenzene oxidation: implication of structure modification. *Appl Catal B Environ* 111–112:476–484. <https://doi.org/10.1016/j.apcatb.2011.10.037>
- Chen W, Koshy P, Adler L, Sorrell CC (2017) Photocatalytic activity of V-doped TiO<sub>2</sub> thin films for the degradation of methylene blue and rhodamine B dye solutions. <https://doi.org/10.1007/s41779-017-0068-0>
- Choi J, Park H, Hoffmann MR (2010) Effects of single metal-ion doping on the visible-light Photoreactivity of TiO<sub>2</sub>. *J Phys Chem C* 114: 783–792. <https://doi.org/10.1021/jp908088x>
- Choi W, Termin A, Hoffmann MR (1994) The role of metal ion dopants in quantum-sized TiO<sub>2</sub>: correlation between photoreactivity and charge carrier recombination dynamics. *J Phys Chem* 98:13669–13679. <https://doi.org/10.1021/j100102a038>
- Colton RJ, Guzman AM, Rabalais JW et al (1978) Electrochromism in some thinfilm transitionmetal oxides characterized by x ray electron spectroscopy Electrochromism in some thin-film transition-metal oxides characterized by x-ray electron spectroscopy, p 409. <https://doi.org/10.1063/1.324349>
- Deng J, Ge Y, Tang C et al (2017) Degradation of ciprofloxacin using A-MnO<sub>2</sub> activated peroxy monosulfate process. Effect of water constituents, degradation intermediates and toxicity evaluation. *Chem Eng J* 330:1390–1400. <https://doi.org/10.1016/j.cej.2017.07.137>
- Dong H, Zeng G, Tang L, Fan C, Zhang C, He X, He Y (2015) An overview on limitations of TiO<sub>2</sub>-based particles for photocatalytic degradation of organic pollutants and the corresponding countermeasures. *Water Res* 79:128–146. <https://doi.org/10.1016/j.watres.2015.04.038>
- El-naas MH, Alhaja MA, Al-zuhair S (2014) Journal of environmental chemical engineering evaluation of a three-step process for the treatment of petroleum refinery wastewater. *J Environ Chem Eng* 2:56–62. <https://doi.org/10.1016/j.jece.2013.11.024>
- Fujishima A, Zhang X, Tryk DA (2008) TiO<sub>2</sub> photocatalysis and related surface phenomena. *Surf Sci Rep* 63:515–582. <https://doi.org/10.1016/j.surfrep.2008.10.001>
- Gallastegi-Villa M, Aranzabal A, Boukha Z, González-Marcos JA, González-Velasco JR, Martínez-Huerta MV, Bañares MA (2015) Role of surface vanadium oxide coverage support on titania for the simultaneous removal of o-dichlorobenzene and NO<sub>x</sub> from waste incinerator flue gas. *Catal Today* 254:2–11. <https://doi.org/10.1016/j.cattod.2015.02.029>
- Ghampson IT, Pecchi G, Fierro JLG, Videla A, Escalona N (2017) Catalytic hydrodeoxygenation of anisole over re-MoO<sub>x</sub>/TiO<sub>2</sub> and re-VO<sub>x</sub>/TiO<sub>2</sub> catalysts. *Appl Catal B Environ* 208:60–74. <https://doi.org/10.1016/j.apcatb.2017.02.047>

- Grabowska E, Reszczyńska J, Zaleska A (2012) Mechanism of phenol photodegradation in the presence of pure and modified-TiO<sub>2</sub>: a review. *Water Res* 46:5453–5471. <https://doi.org/10.1016/j.watres.2012.07.048>
- Greenwood NN, Earnshaw A (1997) Chemistry of the elements, second Edi Harold P. Klug LEA (1974) X-ray diffraction procedures: for polycrystalline and amorphous materials
- He F, Qin K, Luo J, Liu S (2017) Effect of preparation method and vanadium loading amount on the catalytic activity of V/TiO<sub>2</sub> nanoparticles, pp 9050–9055. <https://doi.org/10.1166/jnn.2017.14365>
- Hernández-Alonso MD, Fresno F, Suárez S, Coronado JM (2009) Development of alternative photocatalysts to TiO<sub>2</sub>: challenges and opportunities. *Energy Environ Sci* 2:1231–1257. <https://doi.org/10.1039/b907933e>
- Hidalgo JM, Tišler Z, Kubička D, Raabova K, Bulanek R (2016) (V)/Hydrotalcite, (V)/Al<sub>2</sub>O<sub>3</sub>, (V)/TiO<sub>2</sub> and (V)/SBA-15 catalysts for the partial oxidation of ethanol to acetaldehyde. *J Mol Catal A Chem* 420:178–189. <https://doi.org/10.1016/j.molcata.2016.04.024>
- Hoffmann MR, Martin ST, Choi W, Bahnemann DW (1995) Environmental applications of semiconductor photocatalysis. *Chem Rev* 95:69–96. <https://doi.org/10.1021/cr00033a004>
- Iketani K, De Sun R, Toki M et al (2004) Sol-gel-derived V<sub>x</sub>Ti<sub>1-x</sub>O<sub>2</sub> films and their photocatalytic activities under visible light irradiation. *Mater Sci Eng B Solid-State Mater Adv Technol* 108:187–193. <https://doi.org/10.1016/j.mseb.2003.09.013>
- Jaiswal R, Patel N, Kothari DC, Miotello A (2012) Improved visible light photocatalytic activity of TiO<sub>2</sub> co-doped with vanadium and nitrogen. *Appl Catal B Environ* 126:47–54. <https://doi.org/10.1016/j.apcatb.2012.06.030>
- Kamegawa T, Sonoda J, Sugimura K et al (2009) Degradation of isobutanol diluted in water over visible light sensitive vanadium doped TiO<sub>2</sub> photocatalyst, pp 486:685–688. <https://doi.org/10.1016/j.jallcom.2009.07.035>
- Khan M, Song Y, Chen N, Cao W (2013) Effect of V doping concentration on the electronic structure, optical and photocatalytic properties of nano-sized V-doped anatase TiO<sub>2</sub>. *Mater Chem Phys* 142:148–153. <https://doi.org/10.1016/j.matchemphys.2013.06.050>
- Khodakov A, Olthof B, Bell AT, Iglesia E (1999) Structure and catalytic properties of supported vanadium oxides: support effects on oxidative dehydrogenation reactions. *J Catal* 181:205–216. <https://doi.org/10.1006/jcat.1998.2295>
- Klosek S, Raftery D (2002) Visible light driven V-doped TiO<sub>2</sub> photocatalyst and its photooxidation of ethanol. *J Phys Chem B* 105:2815–2819. <https://doi.org/10.1021/jp004295e>
- Klug HP, Alexander LE (1974) X-Ray diffraction procedures: for polycrystalline and amorphous materials, 2nd edn. Wiley
- Liu B, Wang X, Cai G, Wen L, Song Y, Zhao X (2009) Low temperature fabrication of V-doped TiO<sub>2</sub> nanoparticles, structure and photocatalytic studies. *J Hazard Mater* 169:1112–1118. <https://doi.org/10.1016/j.jhazmat.2009.04.068>
- Loan TT, Long NN (2019) Effect of Co<sup>2+</sup> doping on Raman spectra and the phase transformation of TiO<sub>2</sub>:Co<sup>2+</sup> nanowires. *J Phys Chem Solids* 124:336–342. <https://doi.org/10.1016/j.jpcs.2018.09.007>
- Ma X, Xue L, Yin S, Yang M, Yan Y (2014) Preparation of V-doped TiO<sub>2</sub> photocatalysts by the solution combustion method and their visible light photocatalysis activities. *J Wuhan Univ Technol Mater Sci Ed* 29:863–868. <https://doi.org/10.1007/s11595-014-1010-8>
- Machold T, Suprun WY, Papp H (2008) Characterization of VO<sub>x</sub>-TiO<sub>2</sub> catalysts and their activity in the partial oxidation of methyl ethyl ketone. *J Mol Catal A Chem* 280:122–130. <https://doi.org/10.1016/j.molcata.2007.11.001>
- Martin MV, Villabrille PI, Rosso JA (2015) The influence of Ce doping of titania on the photodegradation of phenol. *Environ Sci Pollut Res* 22:14291–14298. <https://doi.org/10.1007/s11356-015-4667-4>
- Martin ST, Morrison CL, Hoffmann MR (1994) Photochemical mechanism of size-quantized vanadium-doped TiO<sub>2</sub> particles, pp 13695–13704. <https://doi.org/10.1021/j100102a041>
- Martin MV, Ipiña A, Villabrille PI, Rosso JA (2017) Combination of sunlight, oxidants, and Ce-doped TiO<sub>2</sub> for phenol degradation. *Environ Sci Pollut Res* 24:6013–6021. <https://doi.org/10.1007/s11356-016-6258-4>
- McDaniel DH, Brown HC (1957) An Extended Table of Hammett Substituent Constants Based on the Ionization of Substituted Benzoic Acids 23:420–427. <https://doi.org/10.1021/jo01097a026>
- O'Shea KE, Cardona C (1994) Hammett study on the TiO<sub>2</sub>-catalyzed photooxidation of para-substituted phenols. A Kinetic and Mechanistic Analysis *J Org Chem* 59:5005–5009. <https://doi.org/10.1021/jo00096a052>
- Oh S-Y, Shin D-S (2013) Treatment of diesel-contaminated soil by Fenton and persulfate oxidation with zero-valent iron. *Soil Sediment Contam An Int J* 23:180–193. <https://doi.org/10.1080/15320383.2014.808170>
- Palacio M, Rossi L, Fariás Hermosilla EM et al (2017) Selective photodegradation of phenol in the presence of a commercial humic acid. *J Environ Chem Eng* 5:5540–5546. <https://doi.org/10.1016/j.jece.2017.10.021>
- Patel N, Jaiswal R, Warang T, Scarduelli G, Dashora A, Ahuja BL, Kothari DC, Miotello A (2014) Efficient photocatalytic degradation of organic water pollutants using V-N-codoped TiO<sub>2</sub> thin films. *Appl Catal B Environ* 150–151:74–81. <https://doi.org/10.1016/j.apcatb.2013.11.033>
- Plumejeau S, Rivallin M, Brosillon S, Ayral A, Boury B (2016) M-doped TiO<sub>2</sub> and TiO<sub>2</sub>-M<sub>x</sub>O<sub>y</sub> mixed oxides (M = V, bi, W) by reactive mineralization of cellulose - evaluation of their photocatalytic activity. *Eur J Inorg Chem* 2016:1200–1205. <https://doi.org/10.1002/ejic.201501293>
- Princeton University (2016) Office of environmental health and safety, pp 1–2
- Reddy BM, Lee SC, Han DS, Park SE (2009) Utilization of carbon dioxide as soft oxidant for oxydehydrogenation of ethylbenzene to styrene over V<sub>2</sub>O<sub>5</sub>-CeO<sub>2</sub>/TiO<sub>2</sub>-ZrO<sub>2</sub> catalyst. *Appl Catal B Environ* 87:230–238. <https://doi.org/10.1016/j.apcatb.2008.08.026>
- Ren F, Li H, Wang Y, Yang J (2015) Enhanced photocatalytic oxidation of propylene over V-doped TiO<sub>2</sub> photocatalyst: reaction mechanism between V<sup>5+</sup> and single-electron-trapped oxygen vacancy. *Appl Catal B Environ* 176–177:160–172. <https://doi.org/10.1016/j.apcatb.2015.03.050>
- Sacco O, Sannino D, Matarangolo M, Vaiano V (2019) Room temperature synthesis of V-doped TiO<sub>2</sub> and its photocatalytic activity in the removal of caffeine under UV irradiation. <https://doi.org/10.3390/ma12060911>
- Sas OG, Domínguez I, González B, Domínguez Á (2018) Liquid-liquid extraction of phenolic compounds from water using ionic liquids: literature review and new experimental data using [C2mim] FSI. *J Environ Manag* 228:475–482. <https://doi.org/10.1016/j.jenvman.2018.09.042>
- Schneider J, Matsuoka M, Takeuchi M, Zhang J, Horiuchi Y, Anpo M, Bahnemann DW (2014) Understanding TiO<sub>2</sub> photocatalysis: mechanisms and materials. *Chem Rev* 114:9919–9986. <https://doi.org/10.1021/cr5001892>
- Sing KSW, Everett DH, Haul RAW, Moscou L, Pierotti RA, Rouquerol J, Siemieniowska T (1985) Reporting physisorption data for gas/solid systems with special reference to the determination of surface area and porosity 57:603–619. <https://doi.org/10.1351/pac198557040603>
- Song H, Yan L, Ma J, Jiang J, Cai G, Zhang W, Zhang Z, Zhang J, Yang T (2017) Nonradical oxidation from electrochemical activation of peroxydisulfate at Ti/Pt anode: efficiency, mechanism and influencing factors. *Water Res* 116:182–193. <https://doi.org/10.1016/j.watres.2017.03.035>

- Tang T, Lu G, Wang W, Wang R, Huang K, Qiu Z, Tao X, Dang Z (2018) Photocatalytic removal of organic phosphate esters by TiO<sub>2</sub>: effect of inorganic ions and humic acid. *Chemosphere* 206: 26–32. <https://doi.org/10.1016/j.chemosphere.2018.04.161>
- Tolosana-Moranchel A, Ovejero D, Barco B, Bahamonde A, Díaz E, Faraldos M (2019) An approach on the comparative behavior of chloro / nitro substituted phenols photocatalytic degradation in water. *J Environ Chem Eng* 7:103051. <https://doi.org/10.1016/j.jece.2019.103051>
- Wu JCS, Chen CH (2004) A visible-light response vanadium-doped titania nanocatalyst by sol-gel method. *J Photochem Photobiol A Chem* 163:509–515. <https://doi.org/10.1016/j.jphotochem.2004.02.007>
- Yu JH, Nam SH, Lee JW, Kim DI, Boo JH (2019) Oxidation state and structural studies of vanadium-doped titania particles for the visible light-driven photocatalytic activity. *Appl Surf Sci* 472:46–53. <https://doi.org/10.1016/j.apsusc.2018.04.125>
- Zaleska A (2008) Doped-TiO<sub>2</sub>: a review. *Recent Patents Eng* 2:157–164
- Zhang J, Li M, Feng Z, Chen J, Li C (2006) UV raman spectroscopic study on TiO<sub>2</sub>- I. phase transformation at the surface and in the bulk. *J Phys Chem B* 110:927–935. <https://doi.org/10.1021/jp0552473>
- Zhao YF, Li C, Lu S, Yan LJ, Gong YY, Niu LY, Liu XJ (2016) Effects of oxygen vacancy on 3 d transition-metal doped anatase TiO<sub>2</sub>: first principles calculations. *Chem Phys Lett* 647:36–41. <https://doi.org/10.1016/j.cplett.2016.01.040>

**Publisher's note** Springer Nature remains neutral with regard to jurisdictional claims in published maps and institutional affiliations.